Carbon Nanotube Fiber Field Emission Array Cathodes

Steven B. Fairchild, Peng Zhang, Jeongho Park, Tyson C. Back, Daniel Marincel, Zizhuo Huang, and Matteo Pasquali

***Abstract*— Field emission cathodes made from single bulk carbon nanotube (CNT) fibers have demonstrated high emission currents and long lifetimes. This paper investigates the goal of achieving even higher current levels from field emission array (FEA) cathodes comprised of multiple CNT fibers arranged in various array configurations. Arrays were fabricated with 25-μm-diameter CNT fibers in 2-fiber (1 × 2), 4-fiber (2 × 2), and 25-fiber (5 × 5) configurations, and their field emission properties were measured. The 1 × 2 and 2 × 2 FEA cathodes achieved the maximum current values that scaled to greater than 2 mA per emitter. The 5 × 5 FEA cathode achieved a high maximum current value of 22 mA and exhibited stable emission for 10 h at ∼9 mA at an applied field strength of 0.11 V/μm. The Fowler–Nordheim theory was used to calculate the effective field enhancement factor (β_{eff}) values for all of the arrays. Electrostatic simulations were performed using COMSOL Multiphysics modeling software to model the field enhancement of a perfectly uniform 5 × 5 array. The β_{eff} value for the total array was compared to the individual β values at the fiber tips predicted by a surface potential model that predicted the field amplification of all 25 CNT fibers in the array.**

***Index Terms*— Carbon nanotube (CNT), CNT fiber, cathode lifetime, field emission (FE), FE array (FEA).**

I. Introduction

FIELD emission array (FEA) cathodes made from carbon nanotubes (CNTs) have shown considerable promise for use as electron beam sources for vacuum electronic devices [1]–[7]. The applications are many, including X-ray sources [8]–[11], RF sources and amplifiers [12], [13], and electric propulsion devices [14], [15]. These applications require robust FEA cathodes with the ability to emit stable electron beam currents over long time periods. Various approaches have been used to fabricate CNT FEA cathodes, including patterned growth of CNT bundles by chemical vapor deposition on the semiconductor or metallic substrates [16]–[19] and patterned electrophoretic deposition of CNT-based inks [20].

Here, we take a different approach to FEA cathode fabrication by assembling arrays from premade, macroscopic CNT fibers. These highly aligned and densified CNT fibers have proven to be robust field emission (FE) cathodes exhibiting low-voltage operation and long lifetimes [21]–[28].

A single-45-μm-diameter CNT fiber was shown to emit 3 mA for over 10 h at a low applied field strength of 0.2 V/μm [29]. Here, we fabricate CNT fiber FEA cathodes with the goal of achieving a total current that scales to the maximum emission current from a single fiber multiplied by the total number of fibers in the array.

II. Experimental Design

A. CNT Fiber Fabrication

The CNT fibers used for FEA cathode fabrication were made by a wet-spinning technique [30]. The starting material was primarily double-walled CNTs with an uncontrolled distribution of chiralities and types (metallic versus semiconductors), with a diameter of ∼2.4 nm and an aspect ratio of ∼2600–2800 [31]. The aggregated CNTs were mixed with chlorosulfonic acid (CSA) that dissolves CNTs at high concentrations without introducing defects and induces the formation of a liquid crystalline state. This CNT/CSA liquid crystal was then extruded through a small diameter spinneret to create a fiber which was then pulled through coagulant bath to remove the residual acid. The liquid crystalline state of the starting materials facilitates a high degree of CNT alignment along the axial length of the extruded fiber. The fibers are highly aligned and well packed, with high purity and low defect density. This results in high electrical and thermal conductivity, which are key to their excellent performance as both the wire conductors [32] and FE cathodes [29]. Fig. 1 shows the CNT fiber used to build the arrays. They had 25 μm diameter with a room temperature electrical conductivity of 4.64×10^5 S/m and thermal conductivity of 175 W/(mK) as determined by the three-omega method [33].

B. CNT Fiber Work Function Determination

The work function of the CNT fiber was measured experimentally. This experiment consisted of a simulated FE experiment using a hemispherical analyzer on a surface analysis system. The CNT fiber was mounted on a flag style sample holder with the fiber normal to the holder surface. The sample

Manuscript received October 11, 2018; revised January 18, 2019; accepted January 31, 2019. Date of publication March 5, 2019; date of current version May 8, 2019. This work was supported in part by the AirForce Office of Scientific Research under Award FA9550-17RXCOR428, in part by the Air Force Office of Scientific Research Young Investigator Research Program under Award FA9550-18-1-0061, and in part by the AirForce Office of Scientific Research under Award FA9550-18-1-0153 and Award FA9550-15-1-0370. The review of this paper was arranged by Senior Editor S. J. Gitomer. *(Corresponding author: Steven B. Fairchild.)*

S. B. Fairchild, J. Park, and T. C. Back are with the Air Force Research Laboratory, Materials and Manufacturing Directorate, Wright-Patterson Air Force Base, OH 45433 USA (e-mail: steven.fairchild@us.af.mil).

P. Zhang and Z. Huang are with the Department of Electrical and Computer Engineering, Michigan State University, East Lansing, MI 48824-1226 USA.

D. Marincel was with the Department of Chemical and Biomolecular Engineering, Rice University, Houston, TX 77005 USA. He is now with the the Department of Physics and Optical Engineering, Rose-Hulman Institute of Technology, Terre Haute, IN 47803 USA.

M. Pasquali is with the Department of Chemical and Biomolecular Engineering, Rice University, Houston, TX 77005-1892 USA.

Color versions of one or more of the figures in this paper are available online at http://ieeexplore.ieee.org.

Digital Object Identifier 10.1109/TPS.2019.2900219

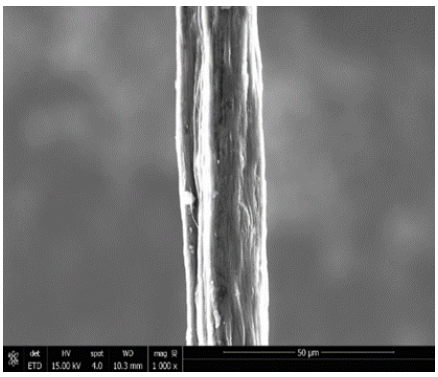

Fig. 1. 25-μm-diameter CNT fiber.

was positioned in front of the analyzer to have a 5-mm gap between the fiber tip and the first lens on the analyzer. The fiber sample was biased at −300 V with the analyzer lens at the ground. Under these conditions, the field strength was sufficient to measure field and secondary emitted electrons from the sample. The data were acquired at a pass energy of 10 eV with 0.05-eV steps. Fig. 2(a) and (b) shows the experimental setup and secondary emission onset used to determine the work function, respectively. The data were fitted with a complementary error function [34] and determined to be 4.65 eV.

C. FEA Cathode Fabrication

CNT fiber was used to fabricate three different FEA cathodes consisting of 2, 4, and 25 fibers. For the 2-fiber (1 × 2) array, CNT fiber segments were cut with a razor blade and mounted to Cu tabs with the conductive silver paint so that 5 mm of fiber was extended above the Cu base. The Cu tabs were 25 mm × 2.5 mm × 1.25 mm and three were stacked together resulting in a 3.75-mm separation between the fibers. Fig. 3(a) shows the 1 × 2 FEA cathode mounted beneath the anode inside the vacuum chamber used for FE measurements. The same method was used for the 4-fiber (2 × 2) array; however, the fiber lengths extending above the Cu tabs were set to 3.5 mm, and two Cu tabs were used to separate the fibers resulting in a spacing of 2.5 mm.

For the 25-fiber (5 × 5) FEA cathode, a sewing technique was used to assist in fabricating an array with uniform spacings. The (5×5) array pattern with 5-mm spacings was marked on a cotton cloth, which was then mounted on a thin graphite sheet with silver paint. Individual fiber segments were sewn through this structure using the array pattern as a guide. The fiber segments were cut to uniform 5 mm height by holding the fibers between two glass slides and cutting with a razor blade across the top. Extra fiber length was left on the underside of the graphite sheet so that each fiber could be contacted to ground. Once all fibers were sewn and cut, silver paint was used to secure the CNT fiber array structure to a Cu block. A diagram of the final array structure is shown in Fig. 3(b). In all three FEA cathodes that were fabricated and tested, each CNT fiber in the array was directly contacted to a piece of bulk Cu with silver paint to assure uniformity of the ground contacts.

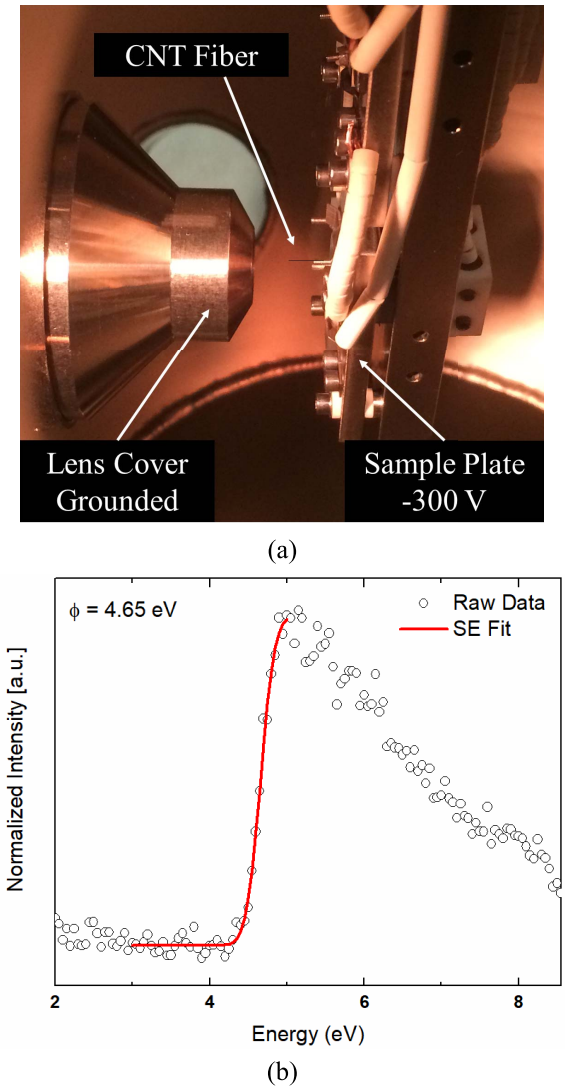

Fig. 2. (a) Image of experimental setup inside the vacuum chamber. The lens cover for the hemispherical analyzer in the X-ray photoelectron spectroscopy system acted as an anode and was at the ground while the sample was negatively biased. The CNT fiber was mounted in the vertical position normal to the sample holder surface. (b) Secondary emission onset from a CNT fiber and curve fit used to determine the work function value of 4.65 eV.

D. Field Emission Measurements

FE measurements were performed in a diode configuration in a custom-designed UHV chamber built by McAllister Technical Services. Measurements were made in a background pressure of 5.0×10^{-9} torr. The anode probe tip is made of stainless steel and is interchangeable to accommodate different size probes. A 7-mm-diameter probe tip was used for the measurements on the 1 × 2 and 2 × 2 arrays, and a 25-mm-diameter probe tip was used for the 5 × 5 array. The probe tip is driven with a stepper motor with a 2.5-μm step size for controlling the anode–cathode (A–K) gap distance. The anode tip was centered over the cathode arrays with an x–y translation stage with the use of two optical cameras directed through viewports positioned at 90° from each other in the same plane. An Infinity SK long-distance microscope was used for imaging the fiber cathode and measuring the distance between the anode and top of the FEA cathodes.

(a)

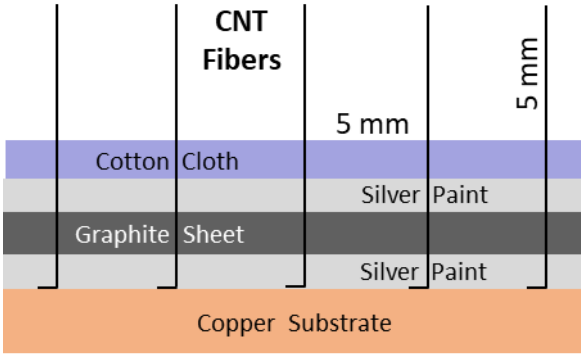

(b)

Fig. 3. (a) Two-fiber (1 × 2) FEA cathode mounted inside the FE measurement vacuum chamber underneath the 7-mm-diameter anode probe. (b) Fabrication process for the 25-fiber (5 × 5) FEA cathode.

A Keithley 2410 sourcemeter was used for providing voltages up to 1 kV and measuring current. For the measurements performed to generate the I–V curves shown in Figs. 4–6, the A–K gap was held constant for each run while the voltage was ramped from 0 to 1 kV at a specified value of the voltage increment per second (V/s). The Keithley 2410 sourcemeter also allows for a current limit to be set and a dwell time to be specified once the current limit is reached. If the target current limit is reached before the voltage reaches 1 kV, then the voltage ramp-up will stop and settle at the value required to maintain the preset current limit value for the specified dwell time. After the preset dwell time at the current limit has expired, the voltage ramps down identically to the V/s rate set for the ramp-up. The voltage is automatically adjusted to maintain the set value of the current. This allowed us to make several measurements on each array and analyze their performance at incremental current levels before reaching the maximum current level that resulted in the failure of the FEA cathode.

The FE measurements for the 1 × 2 FEA cathode were made with a slow voltage ramp-up of 10 V/s to allow for conditioning of the CNT fibers. This allows the fibers to outgas and eliminate surface adsorbates [22]. The A–K

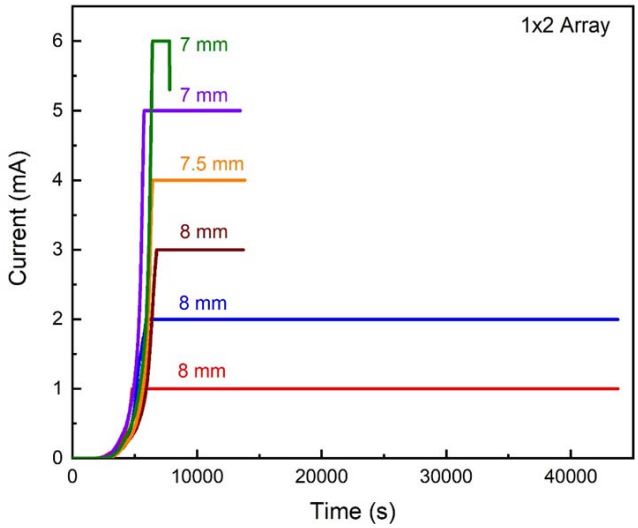

Fig. 4. I–V curves for the 1 × 2 FEA cathode. The A–K gap distance for each run is noted on the I–V curve starting at 8 mm for the current limited run at 1 mA. The gap was eventually lowered to 7 mm where the FEA cathode failed after reaching a current level of 6 mA.

gap distance, which includes the 5-mm fiber height and the distance between the fiber tips and the anode probe, was set to 8.0 mm for the first three I–V measurements. The current limits for these three measurements were set to 1, 2, and 3 mA. The corresponding voltage values (field strengths) required to reach these current limits were 771 V (0.096 V/μm), 885 V (0.110 V/μm), and 963 V (0.120 V/μm). Field strengths were determined by dividing the applied voltage by the A–K gap distance. The dwell time at the maximum current value for the 1- and 2-mA runs was set to 10 h. For the 1-mA run, the voltage drifted up from 771 to 794 V over the 10-h period to maintain the 1-mA current limit. Similarly, for the 2-mA run, the voltage drifted up from 885 to 920 V. For the 3-mA and subsequent runs, the dwell time was reduced to 3 h to limit the potential for cathode heating and failure. For the 4-mA current limited run, the A–K gap was reduced to 7.5 mm, and the maximum voltage (field strength) required to reach this level was 929 V (0.124 V/μm). The A–K gap was further reduced to 7 mm for the runs at 5 and 6 mA, and the maximum voltages (field strengths) for these runs were 863 V (0.123 V/μm) and 929 V (0.133 V/μm), respectively. The cathode eventually failed at 6 mA. The corresponding I–V curves are shown in Fig. 4.

FE measurements for the 2×2 FEA cathode were made with a faster voltage ramp-up rate of 2 V/s to prevent overheating since more current was expected from the larger array. The A–K gap, including the 3.5-mm fiber height, was 6.0 mm for the current limited runs at 5, 6, 7, 8, and 5.5 mm for the 9-mA run. The voltage values (field strengths) required to obtain these current values were 897 V (0.149 V/μm), 920 V (0.153 V/μm), 955 V (0.159 V/μm), 973 V (0.162 V/μm), and 990 V (0.180 V/μm). The dwell time at the maximum current for each run was set to 15 min. The cathode eventually failed at 9 mA. The corresponding I–V curves are shown in Fig. 5.

The 5 × 5 FEA cathode was measured with a faster voltage ramp-up rate of 1 V/s, and the dwell time at the current

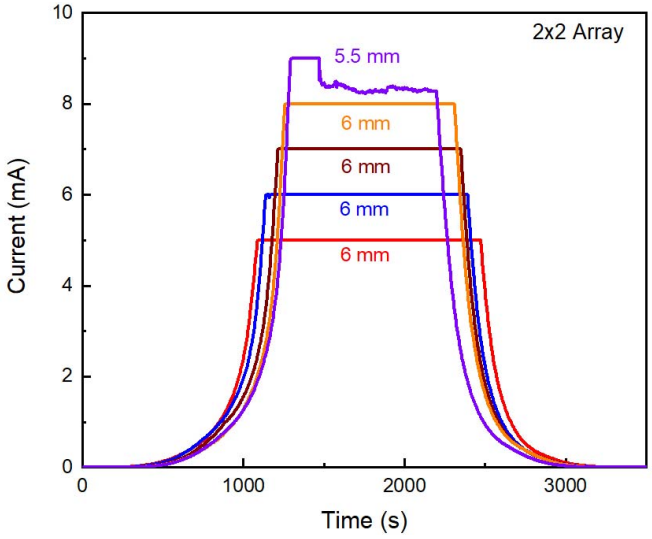

Fig. 5. I–V curves for the 2 × 2 FEA cathode. The A–K gap distance for each run is noted on the I–V curve starting at 6 mm for the current limited run at 5 mA. The gap was eventually lowered to 5.5 mm where the FEA cathode failed after reaching a current level of 9 mA.

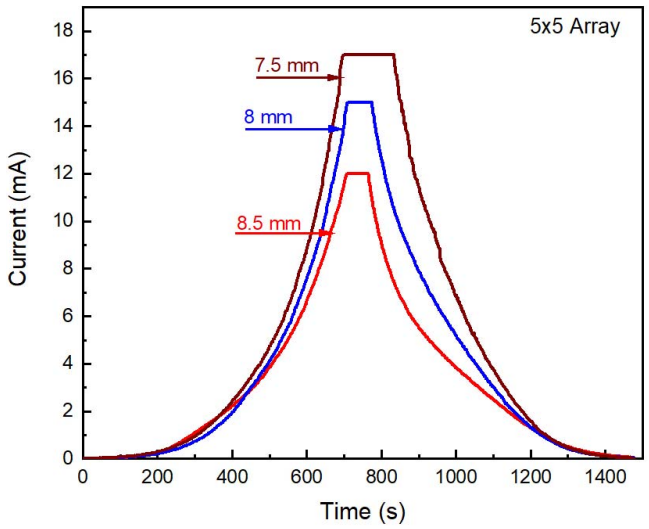

Fig. 6. I–V curves for the 5 × 5 CNT fiber array. The A–K gap distance was initially set to 8.5 mm for the 12-mA curve, and subsequently lowered to 8 mm for the 15-mA curve, and 7.5 mm for the 17-mA curve.

limit was shortened to 100 s due to the higher currents anticipated from the increased number of emitters. The gap distance, including the 5-mm fiber height, was 8.5 mm for the 12-mA current limited run, 8.0 mm at 15 mA, and 7.5 mm at 17 mA. The corresponding voltage values (field strengths) were 976 V (0.1114 V/μm), 977 V (0.122 V/μm), and 975 V (0.130 V/μm). The corresponding I–V curves are shown in Fig. 6.

The 5 × 5 FEA cathode was initially tested for lifetime run with the current limit set to 10 mA. It maintained this level for ~2 h at the maximum voltage level (1 kV) of the sourcemeter. Afterward, the maximum voltage was not high enough to maintain the 10-mA current limit. Therefore, the current slowly started drifting down to a value of ~9 mA at the end of the 10-h run, as shown in Fig. 7. For the final run,

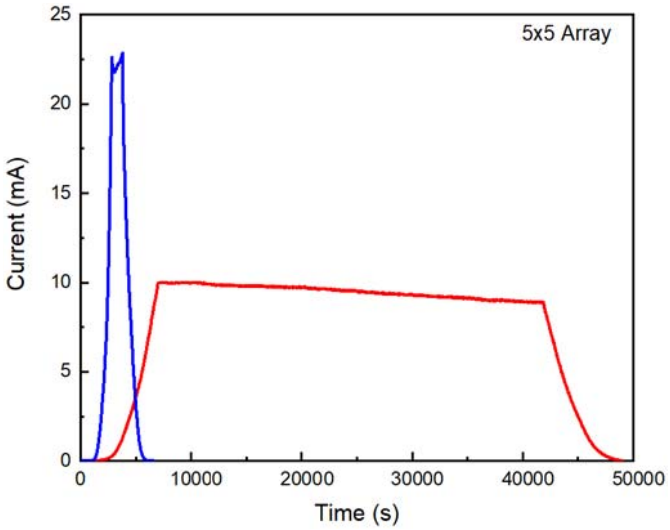

Fig. 7. Blue curve: maximum current run before failure for the 5 × 5 FEA cathode which achieved 22 mA. Red curve: lifetime run of over 10 h starting at an initial current level of 10 mA, which eventually drifted down to 9 mA.

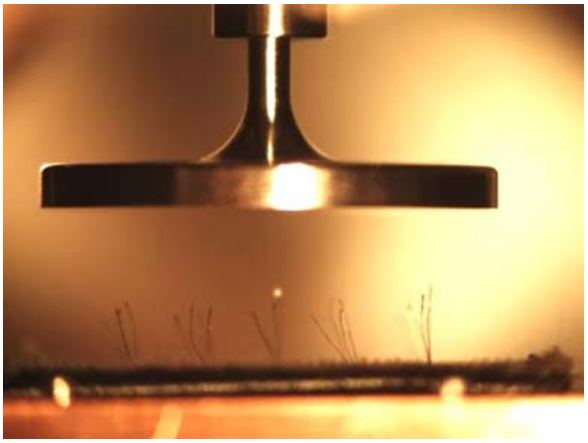

Fig. 8. 25-fiber (5 × 5) FEA cathode mounted inside the FE measurement vacuum chamber underneath the 25-mm-diameter anode probe. The fibers are leaning which creates an uneven height distribution that results in uneven emission currents and a glowing hot spot at the tip of the tallest fiber.

the A–K gap was set to 6.5 mm, and the maximum current reached before failure was 22 mA, which equates to less than 1-mA average emission current per fiber. This is significantly less than the 1 × 2 and 2 × 2 FEA cathodes that failed at current levels equating to greater than 2-mA average current per emitter. This is attributed to the difficulty involved in making a uniform 5 × 5 array. The CNT fibers are not stiff and are, thus, prone to leaning after they are mounted resulting in uneven fiber heights and, therefore, uneven current distribution across all emitters. Imaging of the 5 × 5 array during FE testing showed a hot spot glowing above one fiber that was taller than surrounding fibers, as shown in Fig. 8. This nonuniformity in fiber heights prevented the ability to scale the current up to the maximum expected value of ~50 mA.

Table I summarizes the I–V curves for all of the arrays, including the maximum current, applied field strength, and length of the dwell time at the maximum current for each

TABLE I
CNT FIBER FEA PROPERTIES

Array Size	Current (MA)	Field Strength (V/μm)	Approximate Dwell Time (s)	Current Density (mA/cm^2)
1×2	1.0	0.096	40,000	1,066
	2.0	0.110	40,000	2,133
	3.0	0.120	10,800	3,200
	4.0	0.124	10,800	4,266
	5.0	0.123	10,800	5,333
	6.0	0.133	3,600	6,400
2×2	5.0	0.149	900	80
	6.0	0.153	900	96
	7.0	0.159	900	112
	8.0	0.162	900	128
	9.0	0.180	900	144
5×5	10.0	0.011	40,000	2.50
	12.0	0.114	100	3.00
	15.0	0.122	100	3.75
	17.0	0.130	100	4.25
	22.0	0.221	100	5.50

of the experimental runs. The dwell times are approximate because of the fact that the voltage ramp-up time to the preset current limit is different for each run. Current densities were calculated based on the actual size of the arrays. For the 1×2 array, the total area was 0.009375 cm^2 as determined by the fiber diameter (25 μm) and the separation between emitters (0.375 cm). For current levels above 4 mA, these values are at the best estimations due to increasing emission area for single fiber emission currents greater than 2 mA. This is caused by fiber tip expansion and emission occurring just beneath the fiber tip [29]. The area calculations for the 2×2 and 5×5 arrays were straightforward based on the emitter separations of 2.5 and 5 mm leading total emission areas of 0.0625 and 4 cm^2.

III. THEORY AND MODELING

The FE properties of the fibers were analyzed using the Fowler–Nordheim (FN) theory [35], which relates the current I to the local field F at the emitter surface. The current-gap voltage characteristics could be fitted by the FN equation [23], [27], [36], [37]

$$I(\mathrm{A}) = S_{\mathrm{eff}} A (\beta_{\mathrm{eff}} E)^2 e^{-\frac{B}{\beta_{\mathrm{eff}} E}} \quad (1)$$

where $A = 1.54 \times 10^{-6}/W$, $B = 6.83 \times 10^9 W^{3/2}$, S_{eff} is the effective emission area (m^2), W is the work function (4.65 eV) of the emitting surface, β_{eff} is the effective field enhancement factor, $E = V_g/D$ (in V/m) is the gap electric field, where V_g is the gap voltage, and $D = h + d$ is the gap distance, where h is the fiber height and d is the distance between the fiber tip and the anode probe. In the FN plot, (1) yields a straight line when plotted as $\ln(I/V_g^2)$ versus $1/E$, with the slope of $-B/\beta_{\mathrm{eff}}$. By assuming the gap voltage is the same as the external applied voltage, $V_g = V_{\mathrm{ext}}$ (i.e., no series resistance to the emitter is assumed) [23], [27], the measured FN data

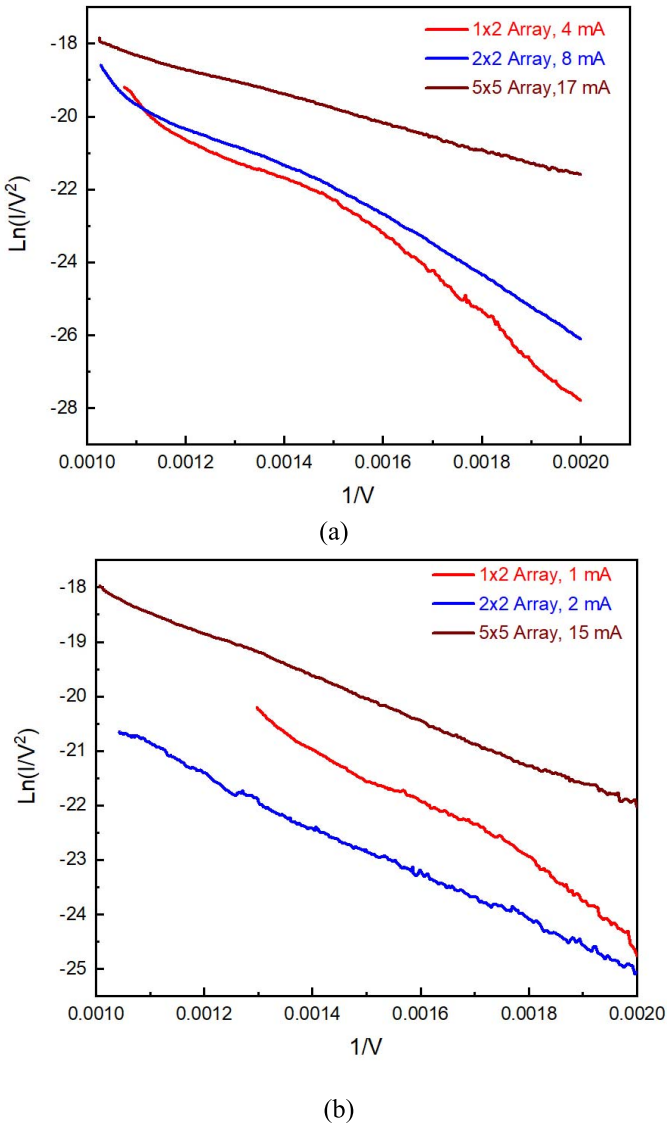

Fig. 9. (a) FN curves for the for 1×2, 2×2, and 5×5 arrays when the average current per emitter was 2 mA, and for the 5×5 array when the average current was 0.7 mA. (b) FN curves for the 1×2, 2×2, and 5×5 arrays when the average current per emitter was 500 mA.

can be fitted by a straight line when the applied voltage is small.

Fig. 9(a) shows the FN curves for the for 1×2, 2×2 and 5×5 arrays when at or near their maximum emission current. The average current per emitter was 2 mA for the 1×2 and 2×2 arrays and 0.68 mA for the 5×5 array. The slope drop in the high electric field regime is most likely caused by the finite series resistance of the fiber emitter in the FE circuit [23]. Joule heating increases at the higher current levels resulting in increased fiber temperature, which can damage the fiber resulting in a pluming effect at the tip and just below [29]. The FN curve for the 5×5 array is more linear than curves for the 1×2 and 2×2 arrays since average current per emitter is significantly less. As a comparison, Fig. 9(b) shows the FN curves for the arrays when the average current per emitter is much less, ~500 μA. The curves are well behaved and closer

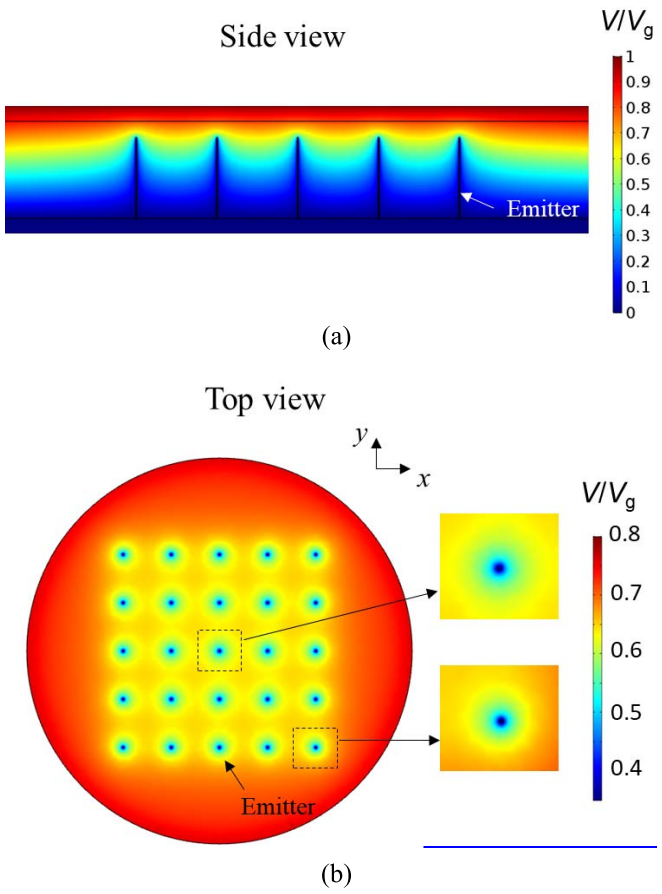

Fig. 10. (a) Side view and (b) top view of the potential profile of the 5×5 FEA cathode calculated from electrostatic simulations using COMSOL.

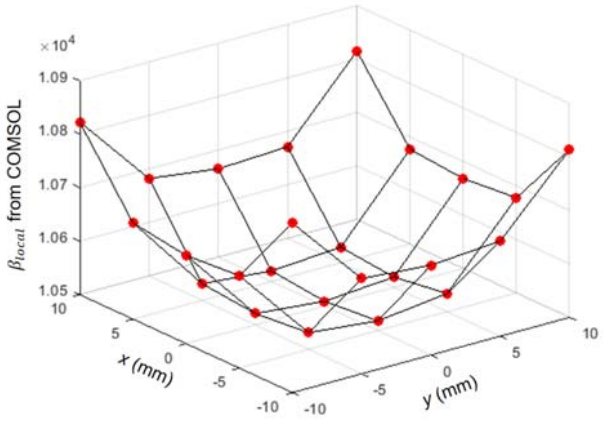

Fig. 11. Corresponding local electric field enhancement factor of the fibers, $\beta_{\text{local}} = E_{\text{local}}/E_0$, defined as the ratio of the local vacuum electric field at the center of the top surface of each tip E_{local} over the applied electric field $E_0 = V_g/D$.

to being linear throughout the entire voltage range. The β_{eff} values calculated from these curves are 1.5×10^5 for 5×5 array, 1.1×10^5 for the 2×2 array, and 9.82×10^4 for the 1×2 array. The 1×2 array still shows the most slope variation which could be due to one fiber emitting more current than the other due to small differences in the height of the CNT fibers resulting in differences in Joule heating between the two fibers.

Electrostatic simulations using COMSOL Multiphysics modeling software were carried out to model the vacuum electric field enhancement of a perfectly uniform 5×5 array, as shown in Fig. 10. In the simulation, the potential and electric fields are calculated by assuming a perfect conducting cathode (including the array of cylindrical emitters) and anode, with the emitter dimensions of height $h = 5$ mm, radius $r = 12$ μm, separation of 5 mm between immediate neighboring emitters, and a tip-to-anode distance of 1 mm.

The potential profiles are shown in Fig. 10(a) and (b). There are strong shielding effects [38] among the neighboring field emitters. The center emitter experiences the strongest shielding effects as it has the largest amount of the surrounding emitters. The potential distribution (and therefore, the electric field distribution) around the emitters at the outer edges of the array becomes asymmetric, as these emitters are shielded by the inner neighboring emitters from one side only. The four emitters at the corners of the array experience the least shielding as they have the least amount of neighboring emitters. Fig. 11 shows the local vacuum electric field enhancement factor, $\beta_{\text{local}} = E_{\text{local}}/E_0$, which is the ratio of the local vacuum electric field at the center of the top surface of each tip E_{local} over the applied electric field $E_0 = V_g/D$, for all the emitter tips in the 5×5 array. It is clear that the local field enhancement factor β_{local} is the largest for the emitters at the corners and the smallest for the center emitter. This indicates that for a uniform array of identical field emitters, the corner emitters would contribute the most of the FE current; on the other hand, the center emitter will emit the least current.

IV. Conclusion

CNT fibers have proven to be robust field emitters that generate high currents at low applied field strengths. The total emission current from small CNT fiber FEA cathodes scale well up to a maximum current that averages 2 mA per fiber. Therefore, larger arrays should be able to produce higher currents; however, the distance between the fiber tips and the anode surface needs to be uniform for the maximum current scaling, which is difficult for the larger arrays due to the lack of stiffness of the CNT fibers. Future work will focus on making more uniform arrays with stiffer fibers, which could be obtained fabricating fibers using longer CNTs [39].

When more uniform FEA cathodes are fabricated, COMSOL simulations have demonstrated that the emission current can be further optimized by varying the fiber heights from the center to the edge of the array, which reduces screening effects. The ultimate goal is to optimize the FEA fabrication process so that large area cathodes up to 100 cm^2 are possible. For these larger arrays, each fiber would have more neighboring fibers resulting in even stronger shielding effects when keeping the spacing fixed. Thus, lower emission current per fiber is expected. The exact value for the limiting current density should depend on the fiber emitter heights and the spacing between them. For larger arrays, since the number of fibers increases, the total current may still increase. For given FEA cathode sizes, the tradeoff between the number of

emitters and the shielding effects (i.e., spacing) can be modeled and optimized. Issues like emission uniformity will also become more important for larger FEA cathode sizes. When eventually fabricated, such large CNT fiber FEA cathodes will be suitable for use as electron beam sources in vacuum electronic devices requiring a high-current, low-voltage operation.

ACKNOWLEDGMENT

The authors would like to thank Dmitri Tsentalovich for providing carbon nanotube fibers.

REFERENCES

[1] Z. Cheng *et al.*, "Field emission cathodes based on structured carbon nanotube arrays," *World J. Res. Rev.*, vol. 4, no. 3, pp. 8–27, Mar. 2017.
[2] V. Chouhan, T. Noguchi, and S. Kato, "Field emission from optimized structure of carbon nanotube field emitter array," *J. Appl. Phys.*, vol. 119, no. 13, Apr. 2016, Art. no. 134303.
[3] F. Giubileo, A. Di Bartolomeo, L. Iemmo, G. Luongo, and F. Urban, "Field emission from carbon nanostructures," *Appl. Sci.*, vol. 8, no. 4, p. 526, 2018.
[4] E. Minoux *et al.*, "Achieving high-current carbon nanotube emitters," *Nano Lett.*, vol. 5, no. 11, pp. 2135–2138, 2005.
[5] Z. Li *et al.*, "High current field emission from individual non-linear resistor ballasted carbon nanotube cluster array," *Carbon*, vol. 89, pp. 1–7, Aug. 2015.
[6] L. F. Velasquez-Garcia, B. Adeoti, Y. Niu, and A. I. Akinwande, "Uniform high current field emission of electrons from Si and CNF FEAs individually controlled by Si pillar ungated FETs," in *IEDM Tech. Dig.*, Dec. 2007, pp. 599–602.
[7] X. Yuan, M. T. Cole, Y. Zhang, J. Wu, M. I. Milne, and Y. Yan, "Parametrically optimized carbon nanotube-coated cold cathode spindt arrays," *Nanomaterials*, vol. 7, no. 1, p. 13, 2017.
[8] A. P. Gupta *et al.*, "Direct synthesis of carbon nanotube field emitters on metal substrate for open-type X-ray source in medical imaging," *Materials*, vol. 10, no. 8, p. 878, 2017.
[9] J.-W. Jeong, J.-W. Kim, J.-T. Kang, S. Choi, S. Ahn, and Y.-H. Song, "A vacuum-sealed compact X-ray tube based on focused carbon nanotube field-emission electrons," *Nanotechnology*, vol. 24, no. 8, 2013, Art. no. 085201.
[10] S. Park *et al.*, "Carbon nanotube field emitters synthesized on metal alloy substrate by PECVD for customized compact field emission devices to be used in X-ray source applications," *Nanomaterials*, vol. 8, no. 6, p. 378, 2018.
[11] B. Sun, Y. Wang, and G. Ding, "Fabrication of high temperature processable CNT array for X-ray generation by micromachining," *Opt. Mater. Exp.*, vol. 7, no. 1, pp. 32–42, 2017.
[12] X. Yuan *et al.*, "A fully-sealed carbon-nanotube cold-cathode terahertz gyrotron," *Sci. Rep.*, vol. 6, Sep. 2016, Art. no. 32936.
[13] W. I. Milne *et al.*, "Aligned carbon nanotubes/fibers for applications in vacuum microwave amplifiers," *J. Vac. Sci. Technol. B, Microelectron.*, Vol. 24, No. 1, Jan./Feb. 2006
[14] L. A. Singh, G. P. Sanborn, S. P. Turano, M. L. R. Walker, and W. J. Ready, "Operation of a carbon nanotube field emitter array in a Hall effect thruster plume environment," *IEEE Trans. Plasma Sci.*, vol. 43, no. 1, pp. 95–102, Jan. 2015.
[15] I. Levchenko, S. Xu, G. Teel, D. Mariotti, M. L. R. Walker, and M. Keidar, "Recent progress and perspectives of space electric propulsion systems based on smart nanomaterials," *Nature Commun.*, vol. 9, p. 879, 2018.
[16] M. T. Cole, K. B. K. Teo, O. Groening, L. Gangloff, P. Legagneux, and W. I. Milne, "Deterministic cold cathode electron emission from carbon nanofibre arrays," *Sci. Rep.*, vol. 4, p. 4840, May 2014.
[17] L. T. Williams, V. S. Kumsomboone, W. J. Ready, and M. L. R. Walker, "Lifetime and failure mechanisms of an arrayed carbon nanotube field emission cathode," *IEEE Trans. Electron. Devices*, vol. 57, no. 11, pp. 3163–3168, Nov. 2010.
[18] S. Sridhar *et al.*, "Enhanced field emission properties from CNT arrays synthesized on inconel superalloy," *ACS Appl. Mater. Interfaces*, vol. 6, no. 3, pp. 1986–1991, 2014.
[19] G. Chen *et al.*, "Low turn-on and uniform field emission from structurally engineered carbon nanotube arrays through growth on metal wire mesh substrates," *Mater. Res. Express*, vol. 4, no. 10, Oct. 2017, Art. no. 105041.
[20] X. Calderón-Colón, H. Geng, B. Gao, L. An, G. Cao, and O. Zhou, "A carbon nanotube field emission cathode with high current density and long-term stability," *Nanotechnology*, vol. 20, no. 32, 2009, Art. no. 325707.
[21] D. Shiffler *et al.*, "Demonstration of an acid-spun single-walled nanotube fiber cathode," *IEEE Trans. Plasma Sci.*, vol. 40, no. 7, pp. 1871–1877, Jul. 2012.
[22] P. T. Murray *et al.*, "Evidence for adsorbate-enhanced field emission from carbon nanotube fibers," *Appl. Phys. Lett.*, vol. 103, no. 5, 2013, Art. no. 053113.
[23] P. Zhang, S. B. Fairchild, T. C. Back, and Y. Luo, "Field emission from carbon nanotube fibers in varying anode-cathode gap with the consideration of contact resistance," *AIP Adv.*, vol. 7, no. 12, 2017, Art. no. 125203.
[24] M. Cahay *et al.*, "Hysteresis during field emission from chemical vapor deposition synthesized carbon nanotube fibers," *Appl. Phys. Lett.*, vol. 105, no. 17, 2014, Art. no. 173107.
[25] M. Cahay, W. Zhu, S. Fairchild, P. T. Murray, T. C. Back, and G. J. Gruen, "Multiscale model of heat dissipation mechanisms during field emission from carbon nanotube fibers," *Appl. Phys. Lett.*, vol. 108, no. 3, Jan. 2016, Art. no. 033110.
[26] S. B. Fairchild *et al.*, "Field emission from laser cut CNT fibers and films," *J. Mater. Res.*, vol. 29, no. 3, pp. 392–402, Feb. 2014.
[27] P. Zhang *et al.*, "Temperature comparison of looped and vertical carbon nanotube fibers during field emission," *Appl. Sci.*, vol. 8, no. 7, p. 1175, 2018.
[28] V. Guglielmotti *et al.*, "Macroscopic self-standing SWCNT fibres as efficient electron emitters with very high emission current for robust cold cathodes," *Carbon*, vol. 52, pp. 356–362, Feb. 2013.
[29] S. B. Fairchild *et al.*, "Morphology dependent field emission of acid-spun carbon nanotube fibers," *Nanotechnology*, vol. 26, no. 10, Feb. 2015, Art. no. 105706.
[30] N. Behabtu *et al.*, "Strong, light, multifunctional fibers of carbon nanotubes with ultrahigh conductivity," *Science*, vol. 339, no. 6116, pp. 182–186, Jan. 2013.
[31] D. E. Tsentalovich *et al.*, "Influence of carbon nanotube characteristics on macroscopic fiber properties," *ACS Appl. Mater. Inter.*, vol. 9, no. 41, pp. 36189–36198, 2017.
[32] X. Wang, N. Behabtu, C. C. Young, D. E. Tsentalovich, M. Pasquali, and J. Kono, "High-ampacity power cables of tightly-packed and aligned carbon nanotubes," *Adv. Funct. Mater.*, vol. 24, no. 21, pp. 3241–3249, Jun. 2014.
[33] L. Lu, W. Yi, and D. L. Zhang, "3ω method for specific heat and thermal conductivity measurements," *Rev. Sci. Instrum.*, vol. 72, no. 7, pp. 2996–3003, 2001.
[34] C. Mathieu *et al.*, "Microscopic correlation between chemical and electronic states in epitaxial graphene on SiC(000^{-}1)," *Phys. Rev. B, Condens. Matter*, vol. 83, no. 23, Jun. 2011, Art. no. 235436.
[35] R. H. Fowler and L. Nordheim, "Electron emission in intense electric fields," *Proc. Roy. Soc. London. Ser. A, Containing Papers Math. Phys. Character*, vol. 119, no. 781, pp. 173–181, May 1928.
[36] R. G. Forbes, "Field emission: New theory for the derivation of emission area from a fowler–nordheim plot," *J. Vac. Sci. Technol. B, Microelectron. Process. Phenom.*, vol. 17, no. 2, pp. 526–533, Mar. 1999.
[37] J. W. Luginsland, A. Valfells, and Y. Y. Lau, "Effects of a series resistor on electron emission from a field emitter," *Appl. Phys. Lett.*, vol. 69, no. 18, pp. 2770–2772, Oct. 1996.
[38] W. Tang, D. Shiffler, K. Golby, M. LaCour, and T. Knowles, "Experimental study of electric field screening by the proximity of two carbon fiber cathodes," *J. Vac. Sci. Technol. B, Microelectron. Process. Phenom.*, vol. 30, no. 6, Nov. 2012, Art. no. 061803.
[39] M. Adnan *et al.*, "Bending behavior of CNT fibers and their scaling laws," *Soft Matter*, vol. 14, no. 41, pp. 8284–8292, 2018.

Authors' photographs and biographies not available at the time of publication.